Collision of dilute suspension of spheres settling in turbulent flow

Johnson Dhanasekaran[1], Anubhab Roy[2] and Donald L. Koch[3]†

[1]Sibley School of Mechanical and Aerospace Engineering,Cornell University, Ithaca, New York 14853, USA

[2]Department of Applied Mechanics, Indian Institute of Technology Madras, Chennai, Tamil nadu 600036, India

[3]Smith School of Chemical and Biomolecular Engineering,Cornell University, Ithaca, New York 14853, USA

(Received xx; revised xx; accepted xx)

Collision of a dilute poly-disperse suspension of sub-Kolmogorov spheres of negligible inertia settling in turbulent flow and interacting through hydrodynamics shaped by breakdown of continuum has been studied for the first time. We study the role of non-Gaussian statistics of turbulent fluctuations on collision rate. To accomplish this we span Reynolds number based on the Taylor micro-scale, including those not accessible through current direct numerical simulation capabilities, using a velocity gradient model and observe a monotonic decrease in collision rate with increasing non-Gaussian intermittency. To this we couple the effects of gravity. We span the parameter space of relative strength of gravity to turbulence, thus observing the non-linear behaviour of the ideal collision rate arising due to the coupling of the two mechanisms. The final component in our study is the interactions between the colliding spheres through uniformly valid hydrodynamic interactions, that includes non-continuum lubrication and full continuum hydrodynamic interactions at larger separations. Hydrodynamic interactions depend on parameters: size ratios of the interacting spheres and Kn=λ_0/a^*, where λ_0 is the mean free path and $a^* = (a_1 + a_2)/2$ is the characteristic length defined by the radii a_1 and a_2 of the two spheres. We span the expanded parameter space and report the retarded collision rate, diminished due to inter-particle interactions, using collision efficiency. To concisely capture the effects of inter-particle interaction we fit the collision efficiency with a fitting function based on a power law in Kn. We have designed the fitting function to explicitly incorporate the relative strength of gravity to turbulence and implicitly capture the size ratio of the interacting spheres with fitting parameters accounting for the rest. This study will provide insight into the collision process relevant to natural systems, such as drop size evolution in clouds, and industrial processes, like carbon black aggregation. In these systems the coupling of gravity and turbulence as well as non-continuum hydrodynamics, the dominant inter-particle interaction in gases, is important for collision dynamics. So, the particle-size evolution and other important aspects of these system can be better understood and more accurately modelled using the results of our study.

1. Introduction

Collisional growth sets particle size evolution in a wide range of systems. In clouds, collisions are the dominant growth mechanism when droplets are moderately large, about 15 μm or larger radii (see Grabowski & Wang 2013). For droplets sizes greater than 40

† Email address for correspondence: dlk15@cornell.edu

μm it is known that the collision process is driven by differential sedimentation. Droplets smaller than 15μm primarily grow by condensation. This leaves the 15-40 μm size range, referred to as the 'size-gap', where it is not fully understood how droplets grow. The current understanding is that turbulence driven collision is important in this regime (Grabowski & Wang 2013). Dynamics in the 'size-gap' will significantly shape the drop size distribution evolution. This drop size distribution informs rain formation as well as the cloud's thermal budget(see Slingo 1990; Peng *et al.* 2002; Feingold *et al.* 1999). So, the study of the macro climate change to our atmosphere is critically dependent on collision rate of water droplets acting under the coupled action of gravity and turbulence. Studying the collision dynamics under this coupled configuration will be the focus of this study.

The turbulence, driving collision in the 'size-gap', is experienced as a linear flow on the sub-Kolmogorov micron-sized droplets that lie in clouds of Kolmogorov length scales of order 1 mm. The Water droplets of interest are typically of radii less than 100 μm. These, due to the nature of the air-water interface, can be modelled as hard spheres. Additionally these droplets interact with each other by disturbing the media. In gaseous media hydrodynamic interaction characterised by a breakdown of continuum in the lubrication regime is expected to be dominant over deformation, inter-facial mobility, or colloidal force over a large particle size range (Sundararajakumar & Koch 1996; Chun & Koch 2005). Thus, collision rate analysis carried out in our study, that couples the differential sedimentation with the stochastic linear flow flow as well as the particles interacting through hydrodynamic interactions shaped by breakdown of continuum, will lead to better predictions of dynamics in the 'size-gap'.

On a smaller environmental scale Niu *et al.* (2016) demonstrated that pollutants near a industrial furnace experience significant aggregation. So, understanding the coagulation process can aid in combating micro-climate pollution. Analysis of coagulation also finds application in industrial setting, such as carbon black aggregation in aerosol reactor(Buesser & Pratsinis 2012). In all these cases the flow is turbulent and the collision dynamics is significantly influenced by gravitational effects. The particles in these examples interact in gaseous media. So, their collision dynamics will be shaped by non-continuum hydrodynamics. So, the results of our study will be applicable to these and other situations beyond cloud physics.

The first treatment of collision in turbulent conditions was carried out by Saffman & Turner (1956). They modelled turbulence experienced by the sub-Kolmogorov particles as a pseudo-steady uni-axial compressional flow and found the collision rate to be $(8\pi/15)^{\frac{1}{2}}(a_1+a_2)^3 n_1 n_2 (\epsilon/\nu)^{\frac{1}{2}}$, where a_1 and a_2 are the radii of the two spheres each with number density n_1, n_2 respectively, ϵ is the dissipation rate of the turbulent flow field, ν is the kinematic viscosity. Even when the background flow is allowed to fluctuate the sub-Kolmogorov particles are expected to experience linear flow at any instant. Using a stochastic linear velocity field multiple studies (see Brunk *et al.* 1997, 1998; Chun & Koch 2005) have calculated the collision rate in turbulent flow. On the other end of the spectrum studies have been carried out on collision under the action of gravity alone (see Smoluchowski 1918; Davis 1984). In studies that do combine gravity and turbulence the calculations are carried out at only limited sizes of the colliding spheres and Reynolds number based on Taylor microscale (Re_λ) due to limitations of direct numerical simulations (see Ayala *et al.* 2008; Li *et al.* 2018). Our result will span all possible sizes and be applicable to the all ranges of Re_λ including the high values, of $O(10^4)$, typical in clouds.

Inter-particle interactions, especially hydrodynamic interactions, play a dominant role in the motion of particles in a medium when particle separation is comparable to their

sizes. However continuum lubrication forces do not allow collision to occur in finite time. One strategy is to underpredict this divergent force to allow collision in finite time (see Ayala *et al.* 2007). However, this does not give collision rates representative of real particles because they collide by overcoming lubrication forces through varous physical mechanisms. In liquid media Van Der Waals plays this crucial role and has been extensively studied in literature (Batchelor & Green 1972; Batchelor 1982; Davis 1984; Wang *et al.* 1994). In gaseous media the breakdown of continuum dominates over deformation, inter-facial mobility, or colloidal force over a large particle size range (Sundararajakumar & Koch 1996; Chun & Koch 2005). Only a few studies consider non-continuum hydrodynamics. However, they are either limited in scope (Chun & Koch 2005, considers only mono-disperse systems) or use the Maxwell slip approximation which is only valid when surface to surface particle separation is much greater than the mean free path (Davis 1984). So, we will use the non-continuum lubrication result by Sundararajakumar & Koch (1996) valid at all separations along with the continuum hydrodynamics at large separations. Using this uniformly valid hydrodynamics result we can calculate the overall collision rate of a dilute poly-disperse suspension of spheres settling in a stochastic turbulent flow. We will also be calculating the ideal collision rate, i.e., without any hydrodynamics, to inform the dynamics arising from turbulence as well as it's coupling with gravity.

Collision dynamics in many systems is predominantly governed by two-body interactions. This is due to low particle volume fraction, about $O(10^{-6})$ (see Balthasar *et al.* 2002; Grabowski & Wang 2013, for carbon black reactor and droplets in clouds respectively). So, three and higher body interactions are neglected in this study.

We neglect the effects of inertia on collision dynamics. Fluid inertia is weak on sub-Kolmogorov scales. In clouds the kolmogorov length scale is about 1 mm (Grabowski & Wang 2013) and the droplets of interest are micron sized. Similarly, in industrial reactors the particles are at most micron sized. The effect of particle inertia on collision rate has been shown to be captured by increasing the local particle concentration (see Sundaram & Collins 1997; Ireland *et al.* 2016; Dhariwal & Bragg 2018). Only when particle response time is significant compared with fluid response does it affect the collision dynamics directly. This is not applicable for most of the droplets smaller than drizzle size (see figure 1 of Ayala *et al.* 2008). Similarly in industrial reactors the particles are typically smaller than 10 μm (Buesser & Pratsinis 2012). Due to the lack of inertia in the system tracking of the evolution of the sphere pairs is accomplished by the mobility formulation. These mobilities take trivial values in the ideal flow and capture the inter-particle interactions when present, thus setting the relative velocity contribution of gravity and turbulence. The overall relative velocity, that determines the motion of the sphere pairs is given by the vector sum of these individual components.

The choice of background turbulent flow field is important for the fidelity of the collision rate calculation. It is numerically too expensive to carry out direct numerical simulation of turbulence. With present capabilities it is not possible to access high enough Taylor's Reynolds number typically encountered in clouds and other systems. So we will use a velocity gradient model to capture the flow experienced by the sub-Kolmogorov particles. The velocity gradient models used by Brunk *et al.* (1998) and Chun & Koch (2005) do not properly capture the non-gaussian nature of turbulent observed in direct numerical simulation. So, we will use the diffusion based velocity gradient model in turbulence developed by Girimaji & Pope (1990). This model will capture important features of turbulence, like the log-normal behaviour of the pseudo-dissipation rate (sum of velocity gradient square) as well as correlation time of the realised straining flow along with the

orientation of vorticity. Thus, velocity gradient models, like the multi-fractal framework proposed by Pereira *et al.* (2018), are superfluous for our purpose.

Collision occurs by a pair of spheres approaching from large separations and colliding. The collision rate is given by the inward flux at contact averaged over all possible starting configurations. For numerical efficiency a time reversed flow is considered and sphere pairs start together and move apart, with the trajectory analysis detecting and rejecting sphere pairs that come back together. Monte-Carlo integration is used to numerically span the initial configurations, in the time-reversed flow, and it is ensemble averaged over the various realisations of the turbulent flow to obtain the collision rate. Due to inter-particle interactions, in addition to the relative velocity, the pair probability, a measure of the local particle concentration relative to the bulk, takes non-trivial values. This pair-probability is an important component in the calculation of collision rate and so it's evolution during the collision event is tracked. The results are expressed through collision efficiency, given as the ratio of overall collision rate with inter-particle interactions to the ideal collision rate where particles do not interact with each other.

Our study is the first to report the variation of collision rate as a function of Reynolds number based on the Taylor micro-scale. Taylor's Reynolds number is a good estimate of the non-Gaussian intermittency of the velocity gradient statistics. We will show how this influences the behaviour of the ideal collision rate as well as the collision efficiency. At this time it is not possible to develop a fully theoretical treatment of variation of collision rate with Taylor's Reynolds number since there is no theory that captures the probability distribution function of the velocity gradients analytically.

In addition to the Taylor's Reynolds number the relative strength of differential-sedimentation to turbulent flow plays an important role in the ideal collision rate. When hydrodynamic interactions are included the relative size of the non-continuum to the interacting spheres and relative size of the interacting spheres play a role. We will span this large parameter space and present important findings. Since it is not feasible to report all of this data we will show results only at a few typical cases and present the important trends. Then we will fit the data for ideal collision rate as well as the collision efficiency and report it. The fitting function for collision efficiency will be constructed based on evolution of a sphere pair in a model system, which in turn will involve integrals of the mobilities in radial space. By cutting off this integral close to the breakdown of continuum we will obtain a function that captures important features of the collision efficiency as a function of the various parameters. This will be adapted to obtain the fitting function we will use. It should be noted that there is no purely theoretical framework for the velocity gradient statistics and so it not possible to incorporate it into our model for the collision efficiency at this point. The collision rate predicted by our study will still capture important aspects of turbulence through the fitted result of the ideal collision rate, which will span a large range of Taylor's Reynolds number.

We will obtain the collision rate for spheres settling in turbulent flow. In §2 we will present the pertinent formulations and outline the procedure we will use to calculate the collision rate. We will present the results for the ideal case, i.e., no interparticle interaction, in §3. We will carry out the calculations with uniformly valid hydrodynamics, that includes non-continuum lubrication and far-field continuum interactions, in §4 and present the collision efficiency. The collision efficiency data spanning a large parameter space will be reported with a fitting function that we will desing in §5. Then in §6 we will discuss important results from our study and how it can be applied to cloud physics.

2. Formulation

In a dilute system the collision of two spheres sets the collision rate K_{ij}, given as,

$$K_{ij} = \frac{dn_i}{dt} = C_{ij} n_i n_j \tag{2.1}$$

n_i is the number density of species i in the bulk. The two species rate constant C_{ij} can be expressed by an area integral as,

$$C_{ij} = -\int_{(r'=a_1+a_2)\&(\mathbf{v}'\cdot\mathbf{n}'<0)} (\mathbf{v}'\cdot\mathbf{n}')P\, dA' \tag{2.2}$$

Here species i has radius a_i moving with relative velocity of $\mathbf{v}'$ when separated by centre to centre distance of r'. In this study as a notational convention we will denote dimensional quantities with prime and their non-dimensional equivalents without it. At radial separation r' the pair probability, P, captures the local species concentration relative to the bulk and it takes non-trivial values due to inter-particle interaction. Contribution to collision rate comes only from the radially inward motion when spheres come into contact with each other. This is captured through $\mathbf{v}'\cdot\mathbf{n}' < 0$, with $\mathbf{n}'$ being the outward normal at the surface on contact.

The equations in our study are scaled with a characteristic length $a^* = (a_1 + a_2)/2$ and a characteristic velocity $\Gamma_\eta(a_1+a_2)/2$, where the Kolmogorov shear rate $\Gamma_\eta = 1/\tau_\eta$, $\tau_\eta = (\epsilon/\nu)^{-\frac{1}{2}}$ is the Kolmogorov time scale, ϵ is the dissipation rate of the turbulent process with ν being the kinematic viscosity. So, the non-dimensional centre to centre distance r ranges from 2 (referred to as collision sphere) to ∞ (where one sphere does not influence the other) while the differential-sedimentation velocity becomes a parameter expressed as $Q = (2\rho g(a_2^2 - a_1^2/[9\mu])/(\Gamma_\eta(a_1+a_2)/2)$, where g is the acceleration due to gravity, ρ is density of the spheres, μ is the dynamic viscosity experienced by the spheres in the medium. The geometrical parameter, the size ratio given as $\kappa = a_2/a_1$, captures the poly-dispersity of the system and has a range of $\kappa \in (0, 1]$. Thus the collision rate can be scaled with $n_1 n_2 \Gamma_\eta (a_1+a_2)^3$ and expressed through an integral over the collision sphere as,

$$\frac{K_{ij}}{n_1 n_2 \Gamma_\eta (a_1+a_2)^3} = -\int_{(r=2)\&(\mathbf{v}\cdot\mathbf{n}'<0)} (\mathbf{v}\cdot\mathbf{n}')P dA \tag{2.3}$$

It should be noted that this formulation and scaling is valid in the absence of any inertia, both the particle and fluid. This is valid for sub-Kolmogorov particles with low particle response time relative to the fluid. In this inertia-less system we use mobility formulation and the non-dimensional relative velocity $\mathbf{v}$ is given as,

$$\begin{aligned} v_i = \Gamma_{ij} r_j - [A(r)\frac{r_i r_j}{r^2} + B(r)(\delta_{ij} - \frac{r_i r_j}{r^2})]\Gamma_{jk} r_k - \\ [L(r)\frac{r_i r_j}{r^2} + M(r)(\delta_{ij} - \frac{r_i r_j}{r^2})]Q\delta_{j3} \end{aligned} \tag{2.4}$$

$A(r), L(r)$ are radial mobilities and $B(r), M(r)$ are tangential mobilities in linear and sedimenting flow respectively. These mobilities capture inter-particle interactions and take trivial values in the ideal flow, i.e., in the absence of particles interacting with each other. Gravity is directed along the negative 3-direction and the other two directions in the cartesian coordinate are degenerate. $\boldsymbol{\Gamma}$ is the velocity gradient of the locally and instantaneously linear turbulent flow experienced by the sub-Kolmogorov spheres which is scaled with the Kolmogorov time scale. $\boldsymbol{\Gamma}$ is obtained from the model developed by Girimaji & Pope (1990) and captures non-Gaussian intermittency, including the log-normal behaviour of the dissipation rate, and important features of the linear flow, such

as correlation time of the straining flow as well as the relative orientation of vorticity, observed in direct numerical simulation of turbulence. We extended the validity of their model to arbitrary Taylor's Reynolds number (Re_λ) by incorporating results for variance of the pseudo-dissipation rate (sum of velocity gradient square) and ratio of integral time scale to Kolmogorov time scale from the published results of Koch & Pope (2002). So this turbulence model is expected to generate velocity gradient statistics with good fidelity, at least pertaining to the collision rate calculation. So it is beyond the scope of this study to include higher order corrections, like those presented by Pereira *et al.* (2018) who use a multi-fractal model for the velocity gradient.

To evaluate the collision rate from equation (2.3) we also need information on P. This can be obtained from the governing equation that can be given as,

$$\frac{\partial P}{\partial t} + \nabla \cdot (\mathbf{v} P) = 0 \tag{2.5}$$

With the boundary condition $P \to 1$ as $r \to \infty$ which corresponds to the particle being too far away to influence each other and all the properties match the bulk value. A non-trivial evolution of the pair-probability is possible only for a non-solenoidal relative velocity. The solenoidal nature of the evolution is broken by inter-particle interactions.

The integrand in equation (2.3) must only include sphere pairs that initially are far away from each other. It is numerically very expensive to evaluate for the case of satellite spheres evolving from r of ∞ to 2 since most of them will miss the test sphere placed at the origin. So, exploiting the Stokes flow reversibility a time-reversed flow is used. In this time-reversed flow the satellite spheres begin at $r = 2$ and those that reach the outer boundary, set as r_∞, without returning to $r = 2$ will have non-zero contributions towards the integral in equation (2.3).

In evaluating equation (2.3) through trajectory analysis in the time-reversed flow all possible locations on the surface of the collision sphere need to be considered. In addition to this the various realisations of the turbulent flow need to be accounted for. So, Monte-Carlo integration is carried out over the initial configurations at one realisation of $\boldsymbol{\Gamma}$ and the collision rate is obtained by an ensemble average over the various of realisations. At any given turbulent flow realisation satellite spheres are generated in intervals of τ_η and $\boldsymbol{\Gamma}$ is updated every $0.1\tau_\eta$ using the velocity gradient model developed by Girimaji & Pope (1990). The satellite spheres evolve with the relative velocity given in equation (2.4). This evolution is numerically carried out through 'ODE45', an in-built adaptive time-stepping routine available in MATLAB. During the evolution satellite spheres do not interact with other satellite sphere in any way. The satellite spheres are allowed to evolve for a long time, upto $150\tau_\eta$. By this time more than %99 of the satellite spheres have either reached $r = 2$ or $r = r_\infty$. To obtain multiple realisations of turbulent flow we take $\boldsymbol{\Gamma}$ separated by long flow times. The correlation time of the straining component of the turbulent flow is $2.3\tau_\eta$ and $7.2\tau_\eta$ for the rotating component of the turbulent flow and integral time scales are about $200\tau_\eta$ even at Re_λ of 2500. So flow times of $400\tau_\eta$ apart is used to obtain a different realisation of the turbulent flow. The error is estimated by calculating the standard deviation across the various realisations used for the ensemble average and reported for one standard error.

3. Ideal collision rate

In the absence of inter-particle interactions $A(r) = 1, L(r) = 0, B(r) = 1, M(r) = 0$ and $P = 1$ everywhere. With the procedure outlined in §2 the collision rate is calculated, with 150 iterations for the Monte-Carlo integration and ensemble averaged over 200

realisations of the turbulent flow. We choose $r_\infty = 7$ as further increases in r_∞ did not significantly alter the collision rate.

The ideal collision rate K_{ij}^0 is presented in figure 1 for the case of $Q = 0$, i.e no effects of gravity included, as a function of the Taylor's Reynolds number. Increasing Re_λ, corresponding to increased intermittency of turublence, causes a dip in the observed collision rate. This behaviour is due to non-Gaussian nature of turbulence and so is not observed in the calculations of Saffman & Turner (1956) who assumed Gaussian statistics for the dissipation rate. Their analysis also assumed a pseudo-steady extensional flow to represent turbulent velocity fields. In this configuration they calculated the collision rate as the inward radial velocity at the collision sphere. To compare with their results we compute the mean inward radial velocity, albeit with a stochastic velocity field that captures the non-Gaussian nature of turbulence, and show it in figure 1, for comparison. This results varies with Re_λ thus demonstrating the role non-Gaussian nature of turbulent statistics plays on collision rate. The collision rate itself, however, is lower than the mean of the inward velocity on the collision sphere since re-circulating trajectories, observed by Brunk *et al.* (1998), decreases the number of successful collision events. Recirculating trajectories arise due to the rotational component as well as the unsteadiness of the linear flow experienced by the spheres. In the time-reversed flow this is seen as satellite spheres returning to the collision sphere. In time-forward flow this corresponds to some trajectories of the satellite spheres from large separation missing the test sphere because of the unsteadiness as well as the rotational component of the linear flow. The rotational component is the dominant driver of the re-circulating trajectories over flow unsteadiness. We test for unsteadiness by performing the collision rate calculation with frozen velocity gradient over the evolution of any given satellite sphere. This results only marginally differs from the full calculation where the velocity field is stochastic over the evolution of the satellite sphere. To analytically obtain the ideal collision rate is beyond the scope of this study. Instead we use a fitting function that is given in equation (3.1) to capture the data that spans the Re_λ parameter space.

The dip in collision rate with increasing Re_λ is directly attributable to the non-Gaussian intermittency of turbulence and our study is the first to report it. A previous study by Ireland *et al.* (2016) considered the inward radial velocity as a function of Re_λ. But they did believe it to be significant. It is possible they reached this conclusion because their highest Re_λ is 597 and, unfortunately, this is at the computational limits of present direct numerical simulation of turbulence. However, only at very high Re_λ can we see significant variation of the collision rate. This strongly supports the hypothesis that the non-Gaussian intermittency of turbulence, which becomes more pronounced at higher Re_λ, leads to the behaviour observed in figure 1. To understand this better we consider the expression used in Pope & Pope (2000) section 6.7 to quantify the tails statistics of the dissipation rate. This is given as,

$$\frac{<\epsilon>^2}{<\epsilon^2>} \approx \mathrm{Re}_\lambda^{-\frac{3}{8}}$$

An equivalent expression in velocity gradient is given as, $\boldsymbol{\Gamma}'\,\mathcal{H}(-\boldsymbol{\Gamma}')/\,<(\boldsymbol{\Gamma}')^2>^{1/2}$, where $\mathcal{H}$ is the Heaviside function. This expression is also expected to depend on Re_λ with a negative exponent and so, by extension, the collision rate as well. At this point it is not possible to analytically arrive at the dependence on the collision rate on Re_λ as there is no fully theoretical model for the velocity gradient in turbulence. So, we will evaluate the exponent by fitting the data to the function shown in equation (3.1).

Figure 2 shows the ideal collision rate K_{ij}^0 as a function of Q. With increasing Q the ideal collision rate increases and converges to a line of slope $(\pi/2)$ and no intercept for

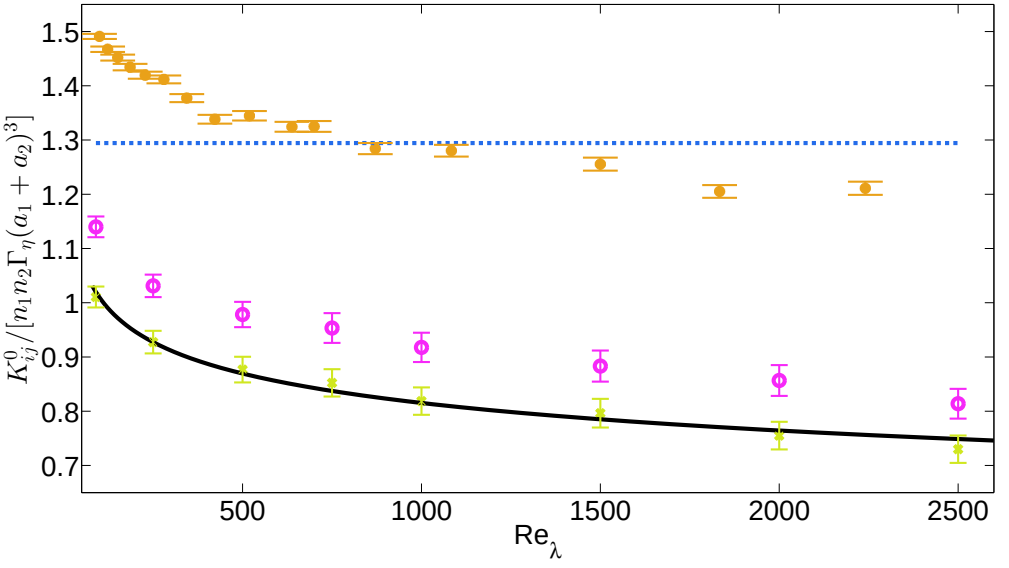

Figure 1: The ideal collision rate K^0_{ij} is given as a function of the Re_λ for $Q = 0$, i.e. no gravitational effects. The error bars coresspond to one standard error. The set of symbols with highest value correspond to the inward velocity on the collision sphere. The set of symbols with intermediate value correspond to persistent turbulence along any given trajectory and stochastic across different trajectories. The set of symbols with the lowest value correspond to the full ideal collision rate calculation where turbulence is stochastic along the trajectory and across different trajectories. The ideal collision rate is fitted with equation (3.1) and represented by the solid line. For reference the calculations by Saffman & Turner (1956) that was performed with pseudo-steady extensional flow and assuming the dissipation rate followed a normal distribution is shown with dashed lines.

all Re_λ. This asymptote corresponds to the ideal pure differential-sedimentation collision rate of $n_1 n_2 \frac{2}{9} \frac{\rho g (a_2^2 - a_1^2)}{\mu} (a_1 + a_2)^2$ calculated by Smoluchowski (1918). The convergence to this result with increasing Q, and the collapse of dependence of the ideal collision rate with Re_λ, is expected as gravity is not a stochastic process and it washes away all the intricacies, like re-circulating trajectories, arising from turbulence. Only $\mathrm{Re}_\lambda = 90$ and 2500 is shown to avoid crowding in the plots. However, the behaviour described here is valid for a large range of Re_λ. To concisely capture the large amount of data we have calculated across the parameter space in Q and Re_λ we use a fitting function. This is given as,

$$\frac{K^0_{ij}}{n_1 n_2 \Gamma_\eta (a_1 + a_2)^3} = \frac{f_1 \mathrm{Re}_\lambda^{f_2}}{1 + f_Q Q} + \frac{\pi}{2} Q$$

Here, f_1, f_2 and f_Q are fitting parameters. This form captures captures asymptotic behaviour in the large Q limit shown in figure 2 as well as the expected power law form for dependence on Re_λ shown in figure 1. We found that $f_1 = 1.55$, $f_2 = -0.09$ and $f_Q = 2.1$ gives best agreement with data. From this expression it is evident the coupling of gravity with turbulence leads to a non-trivial result that cannot be captured through a linear combination of the collision rate of gravity and turbulence.

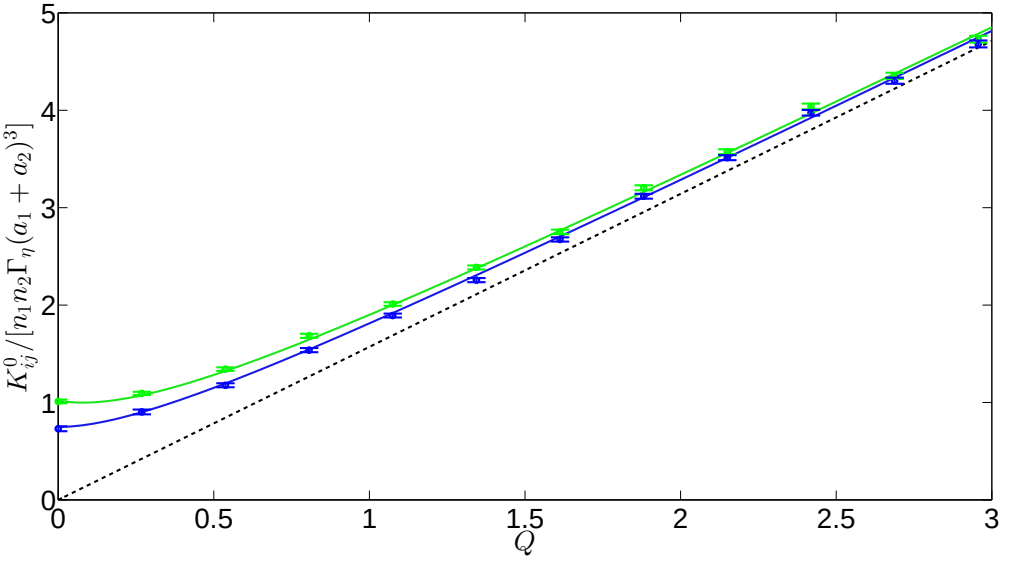

Figure 2: The ideal collision rate K_{ij}^0 is given as a function of Q at only $\mathrm{Re}_\lambda = 90$ and 2500 for sake of conciseness. The symbols correspond to the numerically calculated collision rate and the solid lines to the fit. The higher Re_λ corresponds to lower collision rate. The error bars correspond to one standard error. For reference the ideal collision rate predicted by Smoluchowski (1918) for spheres settling in quiescent flow is given by dashed lines.

4. Collision rate with hydrodynamic interactions

Inter-particle interactions alter the relative velocity, by extension the pair-probability, and lead to a collision rate (K_{ij}^{HI}) that is retarded relative to the ideal flow result. Collision efficiency ($\beta = K_{ij}^{HI}/K_{ij}^0$) will be used to characterise this retardation due to non-continuum hydrodynamics, with the breakdown of continuum parametrised through the Knudsen number, given as $\mathrm{Kn}=\lambda_0/a^*$, where λ_0 is the mean free path. The mobilities capturing this interaction depend only on the centre to centre distance and, more significantly, the important features are sensitive to the surface to surface distance. For this purpose a new radial co-ordinate $\xi = r - 2$ is used. This co-ordinate will also be useful to characterise the pair-probability evolution since it is intricately coupled with the mobilities.

For $\xi \approx O(1)$ far-field continuum hydrodynamics dominates inter-particle interactions. For radial motion the corresponding mobilities are obtained by solving for the velocities in a bispherical coordinate, as presented in the appendix of Wang *et al.* (1994). For $\xi \ll 1$ lubrication forces dominate and the continuum lubrication has been studied by Batchelor & Green (1972). At smaller separations,$\xi \approx O(\mathrm{Kn})$, continuum lubrication breaks down and Sundararajakumar & Koch (1996) calculated the non-continuum lubrication forces. Non-continuum hydrodynamic lubrication weakly diverges, weaker than continuum lubrication, and so allows for collision in finite time. So, we use a uniformly valid radial mobility that spans non-continuum lubrication at very small ξ and smoothly transitions to the far-field continuum hydrodynamic interaction at large ξ through an intermediate continuum lubrication, which acts as the asymptotic behaviour for both of these cases.

For $\xi \approx O(1)$ tangential motion is governed by far-field continuum hydrodynamics and the mobilities are obtained using twin multi-pole solutions. This has been studied by

Jeffrey & Onishi (1984); Jeffrey (1992). They also calculated the near-field continuum hydrodynamics and showed that the tangential mobilities take finite values at contact. This corresponds to the ability of spheres to roll over each other even at contact, thus maintaining non-zero relative velocity at all ξ. This motion will be not be sensitive to Kn. So, $B(r), M(r)$ are set by continuum hydrodynamic interactions at all separations in our study.

Due to the inter-particle interactions, both continuum and non-continuum hydrodynamics, the pair-probability is altered. To calculate the pair-probability evolution along a trajectory we consider equation (2.5) which can be expressed as,

$$\frac{dP}{dt} = -P\,\nabla\cdot\mathbf{v} \tag{4.1}$$

Evaluating this along the trajectory of the satellite sphere gives,

$$P = \exp(-\int \nabla\cdot\mathbf{v}\,dt) \tag{4.2}$$

Here the integrand has the divergence of the relative velocity that is given as,

$$\frac{\partial v_i}{\partial r_i} = -\frac{r_i \Gamma_{ij} r_j}{r}\left[3\,\frac{A(r)-B(r)}{r} + \frac{dA(r)}{dr}\right] - Qs_j\delta_{j3}\left[2\,\frac{L(r)-M(r)}{r} + \frac{dL(r)}{dr}\right] \tag{4.3}$$

It can be seen that the non-solenoidal nature of the relative velocity drives the evolution of the pair-probability. So, as $r\to\infty$ we have $\nabla\cdot\mathbf{v}\to 0$ and have P converge. For this purpose r_∞, outlined in §2, is used to check if the solenoidal nature of the evolution has been reached and we find that $r_\infty = 7$ is sufficient for this purpose.

As the spheres approach each other the relative velocity decays to zero, albeit at the very slow rate of $O(1/\ln[\ln(\mathrm{Kn}/\xi)])$ which allows for collision in finite time. Due to this decay, in the time-reversed flow, numerical issues arise if the satellite spheres begin very close to the test sphere. So it is slightly offset from the collision sphere. The relative velocity and pair probability give finite and convergent value for the integrand in equation (2.3) if the offset is close enough to the collision sphere. An offset of $\xi = 10^{-7}$ is found to give numerically convergent results in our calculation.

With information on the mobilities, by extension the relative velocity and the pair probability, it is possible to evaluate the collision rate through the procedure we described in §2. The calculations span the parameter space in Kn, κ, Q and Re_λ. We perform 50 iterations for the Monte-Carlo integration and ensemble average it over 100 realisations of the turbulent flow, with $r_\infty = 7$. The results, in this section, will be presented in the form of collision efficiency (β).

Figure 3 shows β as a function of Kn at $\kappa = 0.7$ and $\mathrm{Re}_\lambda = 2500$. It can be seen that β decreases as the relative thickness of the continuum breakdown decreases. This is observed across the parameter space. We have shown it here for the $Q = 0$ case (figure 3 (a)) and the $Q\to\infty$ limit (figure 3 (b)). For intermediate values of Q it can be deduced from subsequent figures and not shown here for sake of brevity. This behaviour can be ascribed to the increased continuum lubrication resistance faced by spheres as the relative size of continuum breakdown is smaller. Comparing the two figures it is also evident that the hydrodynamic interaction retards the differential-sedimentation process more than pure turbulence. Both of these qualitative behaviours have been observed at all values κ.

Figure 4 shows β as a function of κ for Kn= 10^{-3} and $\mathrm{Re}_\lambda = 2500$. Just like before

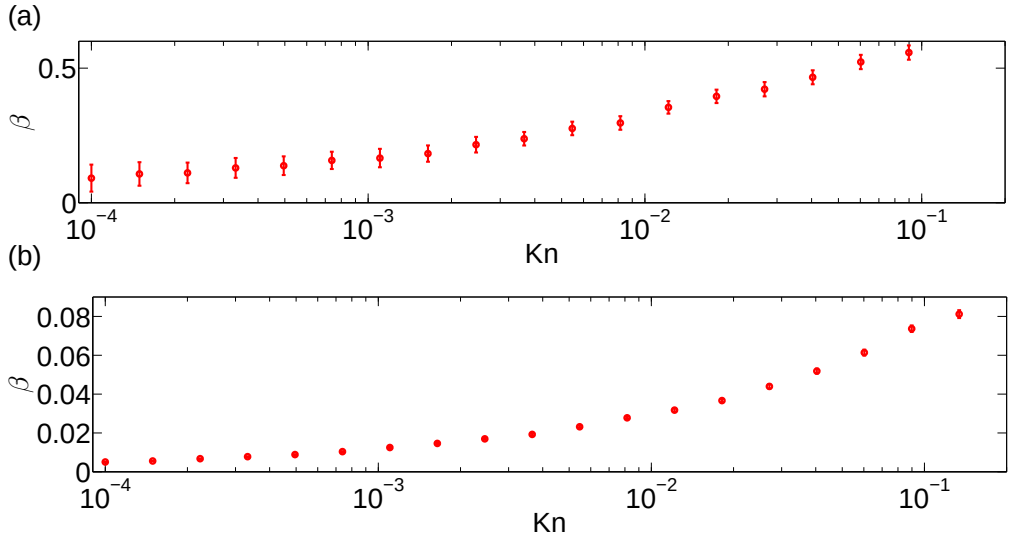

Figure 3: Collision efficiency (β) is plotted as a function of Kn for $\kappa = 0.7$ and $\mathrm{Re}_\lambda = 2500$. Figure (a) is in the pure turbulence limit ($Q = 0$) and figure (b) is in the pure-differential sedimentation limit ($Q \to \infty$). The error bars correspond to one standard error. It can be seen that β decreases with decreasing Kn.

we show results in turbulent dominated flow ($Q = 0$, figure 4 (a)) and note that the efficiency is higher than the gravity dominated regime ($Q \to \infty$, figure 4 (b)). It can be seen in both cases that β decreases as κ decreases. This decrease in β, though not as dramatic as the variation seen with Kn but, is still significant increasing nearly %50 in value from the vastly different spheres to nearly similar ones. Similar sized spheres tend to experience less lubrication forces and, by extension, less resistance to motion as they approach each other, compared to vastly different spheres. So, they have higher efficiency of collision. This behaviour is observed across the parameter space in Kn and Q.

Figure 5 shows the variation of β at Kn$= 10^{-3}$, $\kappa = 0.5$ and $\mathrm{Re}_\lambda = 2500$ as a function of Q. By spanning all ranges of relative strength of gravity to turbulent flow we can observe the monotonic decrease in β with Q. At high Q, i.e., gravity dominated collision process, the far-field hydrodynamic interaction persist for large separations, larger than in the turbulent dominated regime, of $Q \approx 0$. So, in turbulence, motion of interacting spheres is retarded to a lesser extent and reflected in the higher values of β. This effect is true for any linear flow and not just the stochastic linear flow observed by sub-Kolmogorov spheres in turbulence. To demonstrate this, in figure 5, β is also shown for a "persistent" background turbulence, where the trend of decrease in β with increasing Q is seen. For this frozen turbulence we use an uni-axial compressional flow, the most likely realisation in turbulent flow (see Ashurst *et al.* 1987), whose axis of compression is alinged with the direction gravity. For the sake of comparison we have equated the effective strain rate in the frozen linear flow ($\dot{\gamma}$) to the Kolmogorov properties. This equivalent strain rate is obtained by equating the ideal collision rate in static uni-axial compressional flow, calcuated by Zeichner & Schowalter (1977) and given as $[8\pi/(3\sqrt{3})]n_1 n_2 \dot{\gamma}[a_1 + a_2]^3$, with the ideal collision rate predicted by Saffman & Turner (1956), and given to be $(8\pi/15)^{\frac{1}{2}}(a_1 + a_2)^3 n_1 n_2 (\epsilon/\nu)^{\frac{1}{2}}$. This gives the effective shear rate of the frozen linear flow as $\dot{\gamma} = (72/5\pi)^{\frac{1}{2}}(\epsilon/\nu)^{\frac{1}{2}}$ and an equivalent Q is chosen accordingly. It can be seen that the trend of decrease in β with increasing Q is observed in "persistent" turbulence.

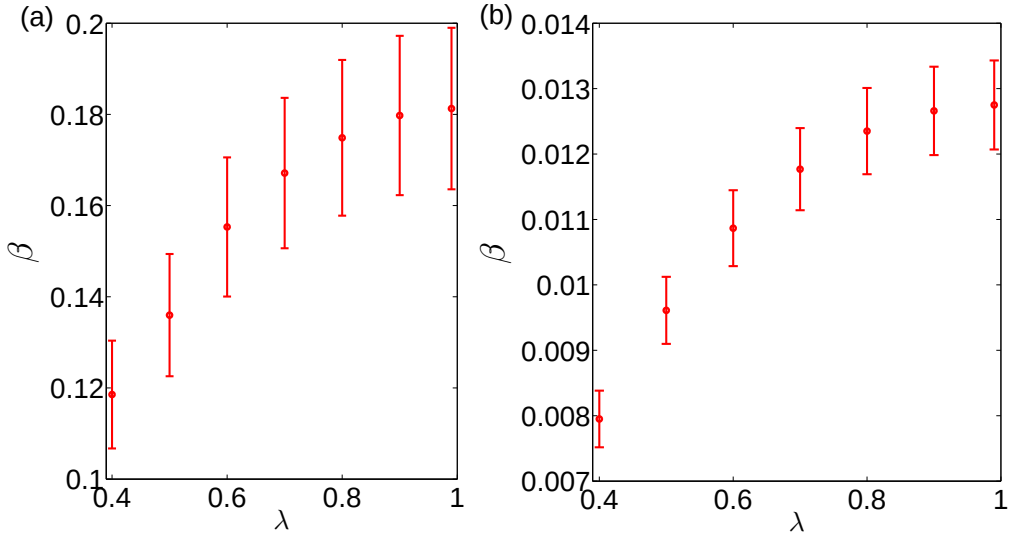

Figure 4: Collision efficiency (β) is plotted as a function of κ for Kn$= 10^{-3}$ and $\mathrm{Re}_\lambda = 2500$. Figure (a) is in the absence of gravitational effects ($Q = 0$) and figure (b) is in a purely gravity driven flow ($Q \to \infty$). The error bars correspond to one standard error. β tends to decrease as the interacting spheres become dissimilar in size.

However, there are some intricate features in the collision efficiency curve that arise due to satellite spheres moving in circuitous trajectories. These effects are washed away by turbulence leading to it having a smoother behaviour. Additionally β, as $Q \to 0$, is higher in stochastic flow field compared to the frozen uni-axial compressional flow and can be ascribed to the role of the various realisations of the linear flow in turbulence, such as the planar shear flow.

Figure 6 shows β for Kn$= 10^{-2}$, $\kappa = 0.9$ as a function of Re_λ for turbulence dominated, turbulence competing with gravity, and gravity dominated regimes. There is no variation of β with Re_λ in the $Q \to \infty$ regime as the gravitationally driven motion washes away any effects of turbulence and Re_λ dependence. At $Q = 0$ we still observe β does not depend on Re_λ since the mobilities do not depend on Re_λ. However, at intermediate Q there is a competition of turbulence with gravity which includes the differing extent by which inter-particle interaction retards the collision rate. This mismatch of the dynamics of the coupled system is directly responsible for the emergence of variation of β with Re_λ at the intermediate values of Q.

5. Fitted form of collision efficiency

In §4 we have presented β at some typical values of Taylor's Reynolds number, size ratio of the spheres, relative strength of gravity to the turbulent flow and strength of non-continuum hydrodynamic interactions. We have presented important qualitative features but it is not feasible to present data on β that exhaustively spans the parameter space. So, we will fit this data and present it this section, along with the motivation for the fitting function. This analytically derived function is based on the important physical characteristics of the pertinent parameters of the collision dynamics: Kn, Q, κ. We have not included Re_λ as there is no fully theoretical understanding of the velocity gradient statistics. Instead we will carry out the analysis at $\mathrm{Re}_\lambda = 2500$, as this is typical in

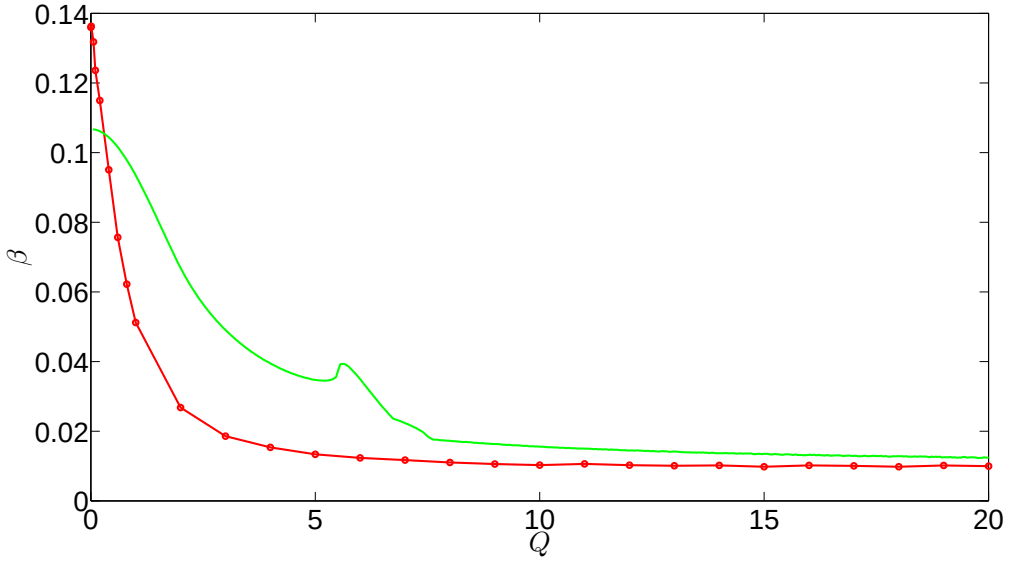

Figure 5: Collision efficiency (β) is plotted as a function of Q for Kn= 10^{-3}, $\kappa = 0.5$. The monotonic curve corresponds to the stochastic linear flow field with $\mathrm{Re}_\lambda = 2500$ and the frozen uni-axial compressional flow, with compression axis aligned with gravity, has kinks at $Q \approx 5$. Error bars are not shown for sake of clarity.

clouds (see Grabowski & Wang 2013). It is to be noted that the variation with Re_λ of β, while statistically significant, does not have as much as influence as other parameters. Additionally non-trivial Re_λ dependence on β occurs only in the $Q \approx 1$ regime. So, important aspects of turbulent fluctuations are captured by the ideal collision rate presented in §3. Including to this the fitted form of the collision efficiency, shown in this section, will give the overall collision rate with high fidelity.

The fitting form for β is motivated by an analytical attempt at calculating the collision efficiency by Batchelor (1982), who considered the evolution of the pair-probability in a purely sedimenting flow. The expression was obtained in the absence of coupling between sedimenting flow with linear flow (that captures turbulence on sub-Kolmogorov scales) by re-writing equation (4.2) as an integral in the radial co-ordinate only. Chun & Koch (2005) used this idea for a linear flow and cut off the lower bound of this integral at ξ =Kn arguing that all the retardation to the collision rate comes from continuum interactions and the integrand does not contribute beyond continuum breakdown. So, they predicted β to show power law in Kn and fitted their results, of a mono-disperse suspension interacting through non-continuum hydrodynamics in turbulent flow, to it. They obtained the exponent from the continuum lubrication forms of the mobilities and the pre-factor was the fitting parameter. We found this simple power law inadequate for our purposes, since it does have a way to incorporate the effects of gravity. So, we build our own fitting function by considering a model system which has frozen uni-axial compressional flow, the most likely linear flow in a turbulent velocity field (see Ashurst *et al.* 1987), coupled with gravity. For this system the pair-probability equation can be written as,

$$\mathbf{v} \cdot \nabla P = -P \nabla \cdot \mathbf{v} \tag{5.1}$$

Next we assume that the model system has the direction of gravity and the compressional

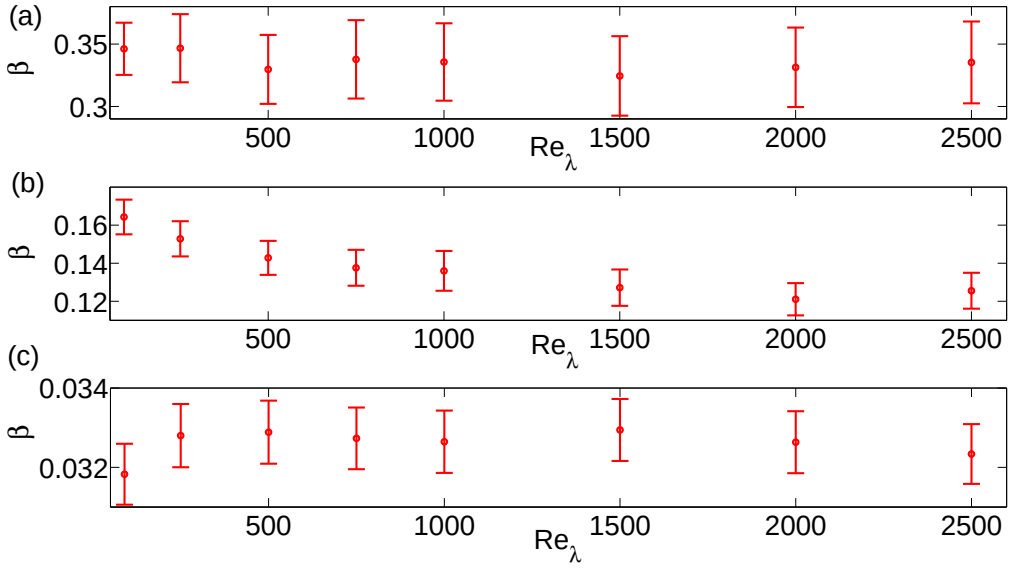

Figure 6: Collision efficiency (β) is plotted as a function of Re_λ for $\mathrm{Kn}= 10^{-2}$, $\kappa = 0.9$ at (a) $Q = 0$, (b) $Q \approx 1$ and (c) $Q \approx 10$. The error bars correspond to one standard error. β varies with Re_λ for moderate Q

axis aligned with each other. At this point it is more convenient to use spherical co-ordinates (r,θ,ϕ), where θ is the polar angle measured from the direction of gravity and ϕ is the azimuthal angle measured in the plane normal to gravity. This plane contains both the extensional axis of the uniaxial compressional flow. For sake of simplicity we will consider the trajectory evolution from a point (θ,0) on the collision sphere. So, the pair-probability equation can be expressed as,

$$v_r \frac{\partial P}{\partial r} + v_\theta \frac{\partial P}{r \partial \theta} = -P \nabla \cdot \mathbf{v} \tag{5.2}$$

Here v_r and v_θ represent velocity in the r and θ direction respectively. Using the method of characteristic on the r derivative and simplifying we get,

$$\int_{r^*}^{\infty} d(\ln\, P) = \int_{r^*}^{\infty} -\frac{\nabla \cdot \mathbf{v}}{v_r} dr \tag{5.3}$$

Here, r^* denotes the lower bound of the integral which will be cut-off before $r = 2$. Expanding $\nabla \cdot \mathbf{v}$ and simplifying we get,

$$\int_{r^*}^{\infty} \frac{\nabla \cdot \mathbf{v}}{v_r} dr = \int_{r^*}^{\infty} d(\ln\, v_r) + \int_{r^*}^{\infty} \left(\frac{2}{r} + \frac{1}{v_r} \frac{1}{r \sin\theta} \frac{\partial (v_\theta \sin\theta)}{\partial \theta} \right) dr \tag{5.4}$$

The relative velocity in spherical co-ordinates can be given as,

$$\begin{aligned} v_r &= r[1 - A(r)](1 - 3\cos^2\theta) - L(r) Q \cos\theta \\ v_\theta &= 3r\,[1 - B(r)] \cos\theta \sin\theta + M(r) Q \sin\theta \end{aligned} \tag{5.5}$$

So, the collision rate can be obtained from equation (5.4) as,

$$\frac{C_{ij}}{\Gamma_\eta (a_1 + a_2)^3} = v_{r,\infty} \exp\Big(\int_{r^*}^{\infty} dr \left[\frac{2}{r} + \frac{3[1 - B(r)](3\cos^2\theta - 1) + 2M(r) Q \cos\theta / r}{r[1 - A(r)](1 - 3\cos^2\theta) - L(r) Q \cos\theta} \right] \Big)$$

Here, $v_{r,\infty}$ is the radial velocity at large separations. To simplify this further we evaluate

κ	A_1	B_0	B_1	L_1	M_0	M_1
0.3	2.53	0.20	3.77	0.45	0.07	1.16
0.4	3.03	0.32	3.46	0.56	0.11	1.16
0.5	3.41	0.42	3.00	0.64	0.15	1.08
0.6	3.69	0.49	2.59	0.70	0.18	0.98
0.7	3.88	0.54	2.28	0.74	0.20	0.89
0.8	4.00	0.57	2.09	0.76	0.21	0.84
0.9	4.06	0.59	1.98	0.78	0.22	0.81
0.99	4.06	0.59	1.95	0.78	0.22	0.80

Table 1: Values of the coefficients of asymptotic forms of the continuum mobilities: $B_0, B_1, M_0, M_1, A, L_1$ at various values of κ. These have been obtained from the work by Jeffrey & Onishi (1984); Jeffrey (1992); Wang *et al.* (1994)

the ideal collision rate for this model system and obtain β. This is given as,

$$\beta = \exp(\int_{\xi^*}^{\infty} d\xi\, [\frac{3[1-B(\xi)](3\cos^2\theta - 1) + M(\xi)Q\cos\theta}{2[1-A(\xi)](1-3\cos^2\theta) - L(\xi)Q\cos\theta} - \frac{3(3\cos^2\theta - 1) + Q\cos\theta}{2(1-3\cos^2\theta) - Q\cos\theta}]) \tag{5.6}$$

Here, we have transformed $\xi = r-2$ for ease of analysis and considered the limit of $\xi \ll 1$. Using the idea that the lower limit of the integral is cut-off when continuum breaks down means we need to know the continuum lubrication forms of the mobilities. From the work of Batchelor & Green (1972) and Batchelor (1982) it is known that $1 - A(\xi) \approx A_1\xi$, $L(\xi) \approx L_1\xi$. For tangential mobilities the work by Jeffrey & Onishi (1984) and Jeffrey (1992) showed that $1 - B(\xi) \approx B_0 + B_1/\ln(\xi^{-1})$, $M(\xi) \approx M_0 + M_1/\ln(\xi^{-1})$. Using these asymptotic forms of the continuum mobilities, whose coefficients $B_0, B_1, M_0, M_1, A_1, L_1$ only depend on κ, and assuming θ does not vary over the domain of integration we evaluate equation (5.6) and set ξ^* =Kn. Thus we get,

$$\beta = p_1 \frac{\mathrm{Kn}^{q_1}}{(p_2 + \ln\frac{1}{\mathrm{Kn}})^{q_2}} \tag{5.7}$$

This will be the fitting function we will use for β. The exponents are given as,

$$q_1 = \frac{3B_0(3\cos^2\theta - 1) + M_0Q\cos\theta}{2A_1(3\cos^2\theta - 1) + L_1Q\cos\theta}$$
$$q_2 = \frac{3B_1(3\cos^2\theta - 1) + M_1Q\cos\theta}{2A_1(3\cos^2\theta - 1) + L_1Q\cos\theta} \tag{5.8}$$

q_1 is associated with the leading order of the tangential lubrication to radial lubrication, while q_2 represents the next term of the tangential lubrication. These depend on the coefficients of the asymptotic forms of the continuum mobilities, which have been given in table 1. p_1 is the upper limit of the integral in equation (5.6), while p_2 represents the fact that the cut-off of the integral at the lower limit need not happen exactly at ξ^* = Kn. p_1 and p_2 along with θ will act as the free parameters in the fitting function.

Figure 7 shows β as a function of Kn for $\kappa = 0.4$ fitted with equation (5.7). Figure 7 (a) shows it at $Q = 0$ and figure 7 (b) in the $Q \to \infty$ regime. It can be seen that the chosen fitting function gives good agreement. The fitted values p_1 and p_2 are shown in table 2 for κ from 0.3 to 0.99. p_1, p_2 have different values depending on the underlying

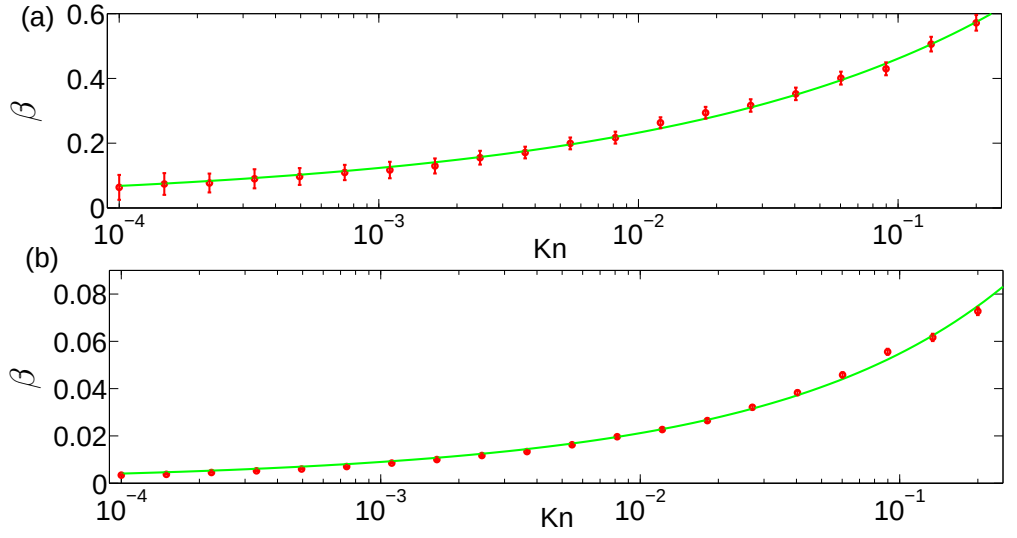

Figure 7: Collision efficiency (β) is plotted as a function of Kn for $\kappa = 0.4$. Figure (a) is in the pure turbulence limit ($Q = 0$) and figure (b) is in the pure-differential sedimentation limit ($Q \to \infty$). The symbols represent the results of the numerical calculation. The error bars correspond to one standard error. The solid line is from the fitting function given in equation (5.7) and they agree well with the results of the numerical calculation.

κ	$p_{1,\epsilon}$	$p_{2,\epsilon}$	$p_{1,g}$	$p_{2,g}$
0.3	89.83	8.11	13.68	5.95
0.4	40.49	8.776	7.99	6.40
0.5	19.27	8.99	4.40	6.71
0.6	12.08	9.54	2.74	6.73
0.7	8.83	9.90	1.97	6.73
0.8	7.39	10.29	1.62	6.73
0.9	6.801	10.64	1.46	6.73
0.99	6.64	10.75	1.42	6.72

Table 2: Values of the fit parameters $p_{1,\epsilon}$, $p_{2,\epsilon}, p_{1g}$ and $p_{2,g}$ at various values of κ

driver of the collision process. So, we denote p_1, p_2 for the pure turbulent flow as $p_{1,\epsilon}$, $p_{2,\epsilon}$ and as $p_{1,g}$, $p_{2,g}$ for pure differential-sedimentation case respectively to avoid ambiguity.

Figure 8 shows β as a function of κ for Kn= 10^{-2} plotted along with equation (5.7). Figure 8 (a) shows it at $Q = 0$ and figure 8 (b) in the $Q \to \infty$ regime. To obtain these curves parameters $p_{1,\epsilon}$, $p_{2,\epsilon}, p_{1g}$ and $p_{2,g}$ are fitted with a polynomial in κ. It can be seen that our numerical simulation data and the output from equation (5.7) agree well with each other.

For any arbitrary Q the fitting parameters p_1 and p_2 in equation (5.7) are expected to take a value somewhere in-between those in the pure turbulent regime and pure differential sedimentation regime. So, we allow $p_1 = p_1(Q)$ and $p_2 = p_2(Q)$ and choose

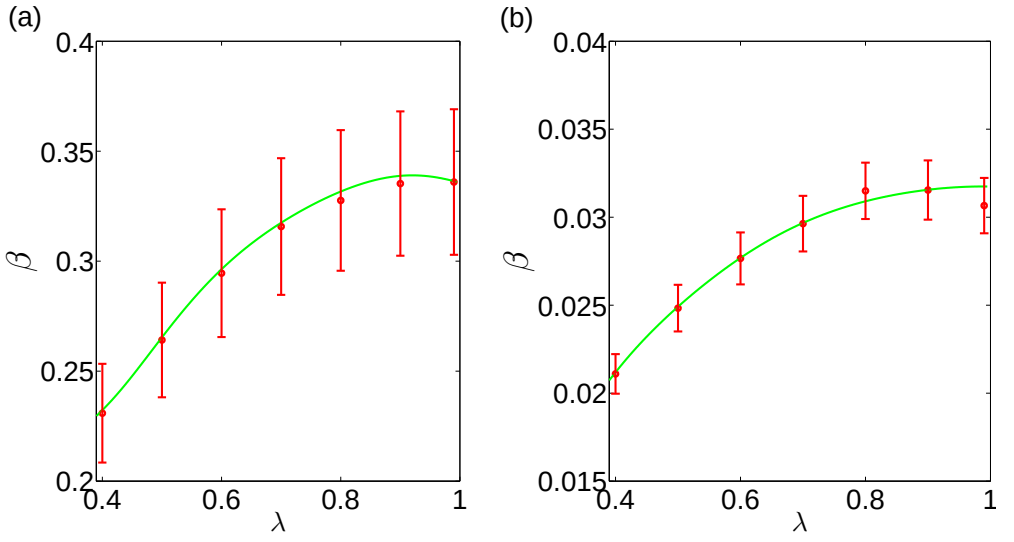

Figure 8: Collision efficiency (β) is plotted as a function of κ at Kn$= 10^{-2}$. Figure (a) is in the absence of gravitational effects ($Q = 0$) and figure (b) is in a purely gravity driven flow ($Q \to \infty$). The symbols represent the results of the numerical calculation with errors bars of one standard error. The solid line is from equation (5.7) agrees well with the data.

the functional form to be,

$$\begin{aligned} p_1(Q) &= \exp(-l_1 Q) p_{1,\epsilon} + [1 - \exp(-l_1 Q)] p_{1,g} \\ p_2(Q) &= \exp(-l_2 Q) p_{1,\epsilon} + [1 - \exp(-l_2 Q)] p_{2,g} \end{aligned} \tag{5.9}$$

The best performance of the fitting function occurs when the remaining free parameters take the values

$$\begin{aligned} \theta &= 50^\circ \\ l_1 &= 1 \\ l_2 &= \frac{\mathrm{Kn} \log_{10}(\frac{1}{\mathrm{Kn}})}{\kappa} \end{aligned} \tag{5.10}$$

Figure 9 shows β as a function of Q for $\kappa = 0.6$ at Kn$= 10^{-3}$ as well as the curve that fits this data. We still use equation (5.7) but with the modified version of the fitting parameters, as given in equation (5.9). The complexity of the fitting function used reflects the underlying complexity of the coupling of the turbulence, gravity and non-continuum driven hydrodynamics.

The fit has been carried out using data on β extensively spanning the parameter space. However, it is not feasible to span all possible values. So, the natural question arises whether it is possible to interpolate the data and achieve good fidelity. To answer this we first look at the qualitative behaviour of β across κ, Q, and Kn and see that they are very similar. This is true of the β data not shown here and so the fit is expected to perform well when spanning the parameter space. Additionally the smooth behaviour of continuum near-field mobility coefficients and the fitting parameters, with respect to κ, gives further credence to the idea that the same qualitative behaviour will observed

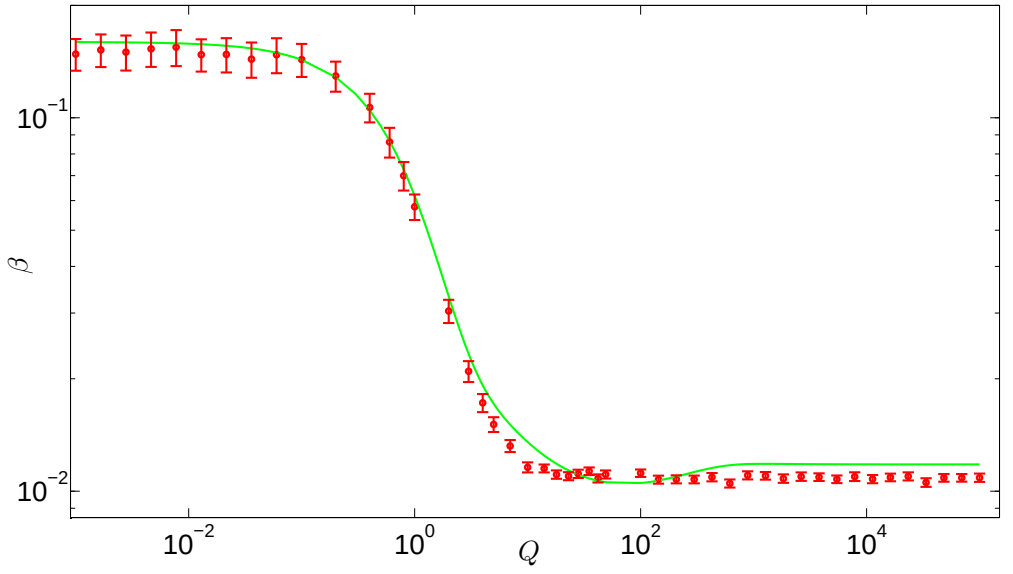

Figure 9: Collision efficiency (β) is plotted as a function of Q for Kn$= 10^{-3}$ for $\kappa = 0.6$. The symbols represent the results of the numerical calculation and the error bars are at one standard error. The solid line is from the modified version of equation (5.7), with fitting parameters given in (5.9). The agreement is good across the parameter space.

across the parameter space and an interpolation of the fitting function will be able to capture β accurately.

6. Discussion

The collision rate, and by extension the collision efficiency, depends on a wide range of parameters. Even without including the effects of gravity we observed decrease in collision rate with increasing Re_λ corresponding to the increasing non-Gaussian intermittency of turbulence. With increasing influence of gravity the collision rate increases with Q and the Re_λ dependence is eventually lost. However, the transition regime is non-trivial and the collision rate cannot be expressed as a linear combination of the pure turbulence and pure differential-sedimentation result.

Including non-continuum hydrodynamics retards the collision rate across the board and the collision efficiency strongly depends on Kn, which captures the extent to which spheres face continuum lubrication before reaching the non-continuum regime. The sedimentation regime still has the higher overall non-dimensional collision rate, but the collision efficiency is significantly lower compared to the pure turbulence regime. This is due to stronger long range hydrodynamic interactions associated with motion driven by an imposed force (the model for gravity-driven motion) compared with sphere motion driven by linear flow (the mode through which sub-Kolmogorov spheres experience turbulence). Due to this differing modes for hydrodynamic interaction, in the transition regime, where gravity and turbulence are competing effects, there is a non-trivial dependence of collision efficiency with Re_λ. This effect is washed away in the $Q \to 0$ and the $Q \to \infty$ regimes. β is also found to decrease as the spheres become more dissimilar in size. This can be understood from table (1) where increasing difference in

size corresponds to a decrease in continuum lubrication mobility, which corresponds to an increase in continuum lubrication resistance force retarding the collision process.

To capture all of the intricate dependencies arising under the action of hydrodynamic interactions a fitting function is carefully designed to fit β. This fitting function does remarkably well and so it is possible to draw some insight from the computed fitting parameters. Of particular interest is p_2 that captures the fact that contribution to collision efficiency from hydrodynamic interactions end exactly at $\xi =$Kn. In fact, large positive values of p_2 across κ strongly indicate that non-continuum regime shapes β to a much larger extent than being a cut-off to lubrication forces.

The results of our study can be used to accurately model the collision-coalescence growth of droplets in clouds. Of particular interest is the 'size-gap', where droplets are too large to grow by condensation but are too small to experience significant gravitational collisional motion. One of the unanswered questions about the 'size-gap' relates to the time taken for rain formation in warm clouds. Experimental studies suggest that drops grow fast, faster than expected from purely gravity driven collision (see Blyth *et al.* 2003; Kolmogorov 1962; Siebert *et al.* 2003; Beard & Ochs III 1993). One potential reason for the slow predicted time to rain formation could be due to condensation, which favours smaller droplets to grow over larger ones, leading to a nearly mono-disperse system at the beginning of the 'size-gap'. Thus models that rely differential-sedimentation driven collision and do not properly account for coupling of it with turbulence will predict unrealistically large characteristic times for collision events. We expect improved prediction of time to rain formation through the use of the physically accurate collision rate result, that properly accounts for the non-continuum lubrication as well as the far-field hydrodynamics with coupling of gravity to linear flow (that captures turbulence on the scale of sub-Kolmorogov particles), performed in our study. Since our study spans a large parameter space in Q, the relative strength of gravity to turbulent flow, it will be adept at resolving the important features of the evolution of the droplet spectra in the 'size-gap' regime where both the gravity and turbulence are expected to be important.

Another issue in the 'size-gap' regime is that drop size distribution is broader than expected from current models (Chaumat & Brenguier 2001). Studies have looked at many mechanisms that can causes broadening (see Lasher-trapp *et al.* 2005; Feingold *et al.* 1999; Cooper *et al.* 2013). However, only a few have looked at collisional growth to account for broadening (see Grabowski & Wang 2009). One reason for not exploring this is because gravity driven collision favours growth of a few large droplets, thus narrowing the distribution. We expect that the features in our collision rate will lead to broadening of droplet spectra since linear flow, stochastic or otherwise, will counteract the tendency towards mono-dispersity that differential sedimentation strongly favours. In addition to this, our results show that the non-continuum hydrodynamics retards differential-sedimentation more than the turbulent flow. We also found that higher Kn, which corresponds to smaller droplet sizes, have higher collision efficiency. It was also observed that nearly similar droplets ($\kappa = 0.99$) show higher collision rate than vastly different droplets ($\kappa = 0.3$). So, the sum total of our results indicate that sedimentation is not as dominant as previously expected and broadening of drop size distribution is more likely to happen (and time to rain formation will be much faster) than what is predicted by current cloud models.

7. Conclusion

Our study is the first to couple the actions of gravity, turbulence and non-continuum hydrodynamics to study the collision rate of a dilute suspension of spheres in an inertia-

less system. We have, for the first time, explored the influence of non-Gaussian tails in turbulence statistics on the collision rate. We have calculated the collision rate that is valid for all size ratios and all relative strength of gravity and turbulence. For the colliding spheres we considered hydrodynamic interactions, including it's behaviour in the non-continuum regime that does not have extensive treatment in literature, and calculated the collision rate over a large parameter space. This included the Taylor's Reynold number, relative strength of gravity to the turbulent flow, the relative size of the mean free path to the size of the interacting spheres, and relative size of the interacting spheres. The retarded collision rate was expressed in terms of collision efficiency and the large amount of data was captured with a carefully designed fitting function.

In §2 we showed the governing equations for collision rate, relative velocity, and pair-probability evolution in a dilute system and presented the scaling used to non-dimensionalise it. We used the mobility formulation for the inertia-less system. The relative velocity consisted of the coupling of differential-sedimenation as well as linear flow, which captures turbulence experienced by sub-Kolmogorov spheres. To capture the stochastic linear flow we used the model for velocity gradient in turbulent flow developed by Girimaji & Pope (1990). This model captures important features of turbulence, like the log-normal behaviour of the dissipation rate as well as the correlation time of straining flow along with the orientation of vorticity relative to it, observed in direct numerical simulation. We then outlined the procedure to obtain the collision rate through a combination of trajectory analysis, Monte-Carlo integration, and ensemble averaging over the various realisations of the turbulent flow.

In §3 we calculated the ideal collision rate using the relative velocity that is solenoidal everywhere and thus the pair-probability takes a trivial values at all spatial locations. The ideal collision rate is first shown in the absence of gravity as a function of the Re_λ, that captures intermittency of turbulence. We showed how the non-Gaussian nature of the velocity gradient statistics plays an important role in the collision rate. We observed the drop in collision rate due to re-circulating trajectories that primarily arises due to the rotational component of the realised linear flow. Then we showed that the inclusion of gravity increases the magnitude of the collision rate and, at the same time, diminishes and eventually removes the variation over Re_λ as well as re-circulation. We span the parameter space in Re_λ and Q and fit the calculated ideal collision rate. We showed the fitting function chosen along with the values of the fit parameters that best capture the large amount of data available. The fitting function demonstrated the complex variation of the ideal collision rate.

In §4 we included the effect of hydrodynamic interactions. We considered the break-down of continuum as the mechanism that allows for collision to occur as, in gaseous media, it dominates over other mechanisms like deformation, inter-facial mobility, and colloidal forces over a large size range. We used the mobilities to capture the uniformly valid hydrodynamic interactions, that includes a non-continuum lubrication as well a full continuum hydrodynamics at larger separation. Using the resulting relative velocity, and by extension the pair-probability, we calculated the collision rate and reported the collision efficiency. We showed the results at a few typical values of the parameter space spanning Kn, κ, Re_λ and Q. We noted the important behaviour over the parameter space such as large values of Kn, turbulence dominated regime, and similar size of the interacting spheres resulting in higher values of β over their respective counterparts. A more non-trivial dependence was observed with Re_λ. With this parameter we showed that β should vary only when gravity and turbulence are competing. We gave brief physical insight into this and other qualitative behaviour observed for β.

In §5 we constructed a fitting function for β to succinctly capture it's variation across

the large parameter space. Important features of Kn, κ and Q on β, observed in the previous section, were built into this fitting function. We presented the details of how we constructed this fitting function, starting with a special trajectory evolution in a model system for which we derived an analytical expression for the collision efficiency. This expression was re-purposed as a fitting function and was able capture the large amount of data with good fidelity. We presented this along with the fit values of all the free parameters.

In §6 we briefly reviewed the results of our study. Then we discussed the application of our model to a cloud system. We discussed how dynamics in 'size-gap' of cloud droplet evolution can be better described using the results of our study. We also touched upon the discrepancy between observed and modelled drop size distribution in the size-gap regime that can potentially be rectified with the more physically realistic collision rate results presented in our study. It was also noted that current understanding of the relative importance of mechanisms in the dynamics of cloud evolution, such as the relative strength of differential-sedimentation driven coalescence with respect to turbulence driven coalescence, would need to be re-evaluated based on conclusions our study.

Acknowledgement

This work was supported by NSF grant 1435953

REFERENCES

Ashurst, Wm T, Kerstein, AR, Kerr, RM & Gibson, CH 1987 Alignment of vorticity and scalar gradient with strain rate in simulated navier–stokes turbulence. *The Physics of fluids* **30** (8), 2343–2353.

Ayala, Orlando, Grabowski, Wojciech W & Wang, Lian-Ping 2007 A hybrid approach for simulating turbulent collisions of hydrodynamically-interacting particles. *Journal of Computational Physics* **225** (1), 51–73.

Ayala, Orlando, Rosa, Bogdan, Wang, Lian-Ping & Grabowski, Wojciech W 2008 Effects of turbulence on the geometric collision rate of sedimenting droplets. part 1. results from direct numerical simulation. *New Journal of Physics* **10** (7), 075015.

Balthasar, Michael, Mauss, Fabian, Knobel, A & Kraft, M 2002 Detailed modeling of soot formation in a partially stirred plug flow reactor. *Combustion and Flame* **128** (4), 395–409.

Batchelor, GK 1982 Sedimentation in a dilute polydisperse system of interacting spheres. part 1. general theory. *Journal of Fluid Mechanics* **119**, 379–408.

Batchelor, GK & Green, J-T_ 1972 The hydrodynamic interaction of two small freely-moving spheres in a linear flow field. *Journal of Fluid Mechanics* **56** (2), 375–400.

Beard, Kenneth V & Ochs III, Harry T 1993 Warm-rain initiation: An overview of microphysical mechanisms. *Journal of Applied Meteorology* **32** (4), 608–625.

Blyth, Alan M, Lasher-Trapp, Sonia G, Cooper, William A, Knight, Charles A & Latham, John 2003 The role of giant and ultragiant nuclei in the formation of early radar echoes in warm cumulus clouds. *Journal of the atmospheric sciences* **60** (21), 2557–2572.

Brunk, Brett K, Koch, Donald L & Lion, Leonard W 1997 Hydrodynamic pair diffusion in isotropic random velocity fields with application to turbulent coagulation. *Physics of Fluids* **9** (9), 2670–2691.

Brunk, Brett K, Koch, Donald L & Lion, Leonard W 1998 Turbulent coagulation of colloidal particles. *Journal of Fluid Mechanics* **364**, 81–113.

Buesser, Beat & Pratsinis, Sotiris E 2012 Design of nanomaterial synthesis by aerosol processes. *Annual review of chemical and biomolecular engineering* **3**, 103–127.

Chaumat, Laure & Brenguier, Jean-Louis 2001 Droplet spectra broadening in cumulus

clouds. part ii: Microscale droplet concentration heterogeneities. *Journal of the atmospheric sciences* **58** (6), 642–654.

Chun, J & Koch, DL 2005 Coagulation of monodisperse aerosol particles by isotropic turbulence. *Physics of Fluids* **17** (2), 027102.

Cooper, William A, Lasher-Trapp, Sonia G & Blyth, Alan M 2013 The influence of entrainment and mixing on the initial formation of rain in a warm cumulus cloud. *Journal of the Atmospheric Sciences* **70** (6), 1727–1743.

Davis, Robert H 1984 The rate of coagulation of a dilute polydisperse system of sedimenting spheres. *Journal of Fluid Mechanics* **145**, 179–199.

Dhariwal, Rohit & Bragg, Andrew D 2018 Small-scale dynamics of settling, bidisperse particles in turbulence. *Journal of Fluid Mechanics* **839**, 594–620.

Feingold, Graham, Cotton, William R, Kreidenweis, Sonia M & Davis, Janel T 1999 The impact of giant cloud condensation nuclei on drizzle formation in stratocumulus: Implications for cloud radiative properties. *Journal of the atmospheric sciences* **56** (24), 4100–4117.

Girimaji, SS & Pope, SB 1990 A diffusion model for velocity gradients in turbulence. *Physics of Fluids A: Fluid Dynamics* **2** (2), 242–256.

Grabowski, Wojciech W & Wang, L-P 2009 Diffusional and accretional growth of water drops in a rising adiabatic parcel: effects of the turbulent collision kernel. *Atmospheric Chemistry and Physics* **9** (7), 2335–2353.

Grabowski, Wojciech W & Wang, Lian-Ping 2013 Growth of cloud droplets in a turbulent environment. *Annual review of fluid mechanics* **45**, 293–324.

Ireland, Peter J, Bragg, Andrew D & Collins, Lance R 2016 The effect of reynolds number on inertial particle dynamics in isotropic turbulence. part 2. simulations with gravitational effects. *Journal of Fluid Mechanics* **796**, 659–711.

Jeffrey, DJ 1992 The calculation of the low reynolds number resistance functions for two unequal spheres. *Physics of Fluids A: Fluid Dynamics* **4** (1), 16–29.

Jeffrey, DJ & Onishi, Y 1984 Calculation of the resistance and mobility functions for two unequal rigid spheres in low-reynolds-number flow. *Journal of Fluid Mechanics* **139**, 261–290.

Koch, Donald L & Pope, Stephen B 2002 Coagulation-induced particle-concentration fluctuations in homogeneous, isotropic turbulence. *Physics of Fluids* **14** (7), 2447–2455.

Kolmogorov, Andrey Nikolaevich 1962 A refinement of previous hypotheses concerning the local structure of turbulence in a viscous incompressible fluid at high reynolds number. *Journal of Fluid Mechanics* **13** (1), 82–85.

Lasher-trapp, Sonia G, Cooper, William A & Blyth, Alan M 2005 Broadening of droplet size distributions from entrainment and mixing in a cumulus cloud. *Quarterly Journal of the Royal Meteorological Society: A journal of the atmospheric sciences, applied meteorology and physical oceanography* **131** (605), 195–220.

Li, Xiang-Yu, Brandenburg, Axel, Svensson, Gunilla, Haugen, Nils EL, Mehlig, Bernhard & Rogachevskii, Igor 2018 Effect of turbulence on collisional growth of cloud droplets. *Journal of the Atmospheric Sciences* **75** (10), 3469–3487.

Niu, Hongya, Cheng, Wenjing, Pian, Wei & Hu, Wei 2016 The physiochemical properties of submicron particles from emissions of industrial furnace. *World Journal of Engineering* **13** (3), 218–224.

Peng, Yiran, Lohmann, Ulrike, Leaitch, Richard, Banic, Catharine & Couture, Mark 2002 The cloud albedo-cloud droplet effective radius relationship for clean and polluted clouds from race and fire. ace. *Journal of Geophysical Research: Atmospheres* **107** (D11), AAC–1.

Pereira, Rodrigo M, Moriconi, Luca & Chevillard, Laurent 2018 A multifractal model for the velocity gradient dynamics in turbulent flows. *Journal of Fluid Mechanics* **839**, 430–467.

Pope, Stephen B & Pope, Stephen B 2000 *Turbulent flows*. Cambridge university press.

Saffman, PGf & Turner, JS 1956 On the collision of drops in turbulent clouds. *Journal of Fluid Mechanics* **1** (1), 16–30.

Siebert, Holger, Wendisch, Manfred, Conrath, Thomas, Teichmann, Ulrich &

Heintzenberg, Jost 2003 A new tethered balloon-borne payload for fine-scale observations in the cloudy boundary layer. *Boundary-layer meteorology* **106** (3), 461–482.

Slingo, A 1990 Sensitivity of the earth's radiation budget to changes in low clouds. *Nature* **343** (6253), 49.

Smoluchowski, M v 1918 Versuch einer mathematischen theorie der koagulationskinetik kolloider lösungen. *Zeitschrift für physikalische Chemie* **92** (1), 129–168.

Sundaram, Shivshankar & Collins, Lance R 1997 Collision statistics in an isotropic particle-laden turbulent suspension. part 1. direct numerical simulations. *Journal of Fluid Mechanics* **335**, 75–109.

Sundararajakumar, RR & Koch, Donald L 1996 Non-continuum lubrication flows between particles colliding in a gas. *Journal of Fluid Mechanics* **313**, 283–308.

Wang, Hua, Zinchenko, Alexander Z & Davis, Robert H 1994 The collision rate of small drops in linear flow fields. *Journal of fluid mechanics* **265**, 161–188.

Zeichner, GR & Schowalter, WR 1977 Use of trajectory analysis to study stability of colloidal dispersions in flow fields. *AIChE Journal* **23** (3), 243–254.